MAP-MRI revisited: Shorter acquisitions, fast propagator anisotropy estimation, new contrasts.

Deneb Boito[1], Alexandru V. Avram[2], Magnus Herberthson[1,3], Peter J. Basser[2], and Evren Özarslan[1,4]
[1]Spin Nord AB, Linköping, Sweden, [2]Section on Tissue Biophysics and Biomimetics, NICHD, National Institutes of Health, Bethesda, MD, United States, [3]Department of Mathematics, Linköping University, Linköping, Sweden, [4]Department of Biomedical Engineering, Linköping University, Linköping, Sweden

Synopsis

Motivation: To advance the clinical translation of MAP-MRI.

Goal(s): To accelerate MAP-MRI data acquisition using advanced data processing, to describe novel microstructural contrasts, and to shorten MAP-MRI processing/analysis times.

Approach: A recently developed constrained propagator estimation framework was employed to derive MAP-MRI parameters from simulated efficient data acquisitions. Novel metrics and processing methods were proposed and tested on a public dataset.

Results: The proposed estimation framework obviates the need for extensive data collection, while the novel metrics could provide additional insights when assessing different diseases, thus advancing the clinical translation and application of MAP-MRI.

Impact: This work shows that sophisticated postprocessing reduces the number of diffusion encodings needed for MAP-MRI. Together with the proposed novel contrasts, these advances should facilitate neuroimaging studies employing MAP-MRI and possibly enable new clinical applications.

Introduction

Mean Apparent Propagator (MAP)-MRI[1] is an imaging technique which quantifies the distribution of spins' net displacements from multiple diffusion MRI (dMRI) measurements. Several works have demonstrated the clinical potential of quantities obtained via MAP-MRI[2-8]. Recent developments have made it possible to strictly enforce positivity constraints in the estimation of the propagator[9]. Here, we assess whether enforcing positivity constraints enables the accurate estimation of MAP-MRI microstructural parameters from fewer dMRI volumes, which is critical for the method's clinical applicability[10]. In addition, we propose several novel metrics, and a fast method for obtaining the propagator anisotropy.

Theory

MAP-MRI

In MAP-MRI, the diffusion-weighted signal and the mean propagator are represented using a series of orthogonal basis functions in the local anatomical frame-of-reference[1]:

$$E(\mathbf{q}) = \mathbf{a}^t \mathbf{\Phi}(\mathbf{q}) \qquad \leftrightarrow \qquad \mathrm{FT} \qquad \leftrightarrow \qquad P(\mathbf{r}) = \mathbf{a}^t \mathbf{\Psi}(\mathbf{r})$$

where $\mathbf{q}$ is the q-vector, $\mathbf{\Phi}$ and $\mathbf{\Psi}$ represent the basis functions in q-space and displacement-space, respectively, and $\mathbf{a}$ is the vector containing the coefficients for the basis terms.
For symmetric propagators, the number of coefficients to be estimated is

$$\frac{(N_{\max}+2)(N_{\max}+4)(2N_{\max}+3)}{24}$$

,
where $N_{\max} = n_1 + n_2 + n_3$ defines the radial order of the expansion, and n_1, n_2, n_3 index the basis functions.

NOVEL METRICS

Microstructure descriptors can be obtained by quantifying the distance between different propagators[1]. For example, the Non-Gaussianity (NG) index is computed as

$$NG = \sqrt{1 - \frac{\langle \mathcal{P}_0, \mathcal{P}_{N_{\max}} \rangle}{\langle \mathcal{P}_{N_{\max}}, \mathcal{P}_{N_{\max}} \rangle}}$$

where $\mathcal{P}_0$ is the Gaussian propagator, and

$$\langle \mathcal{P}(\mathbf{r}), \mathcal{Q}(\mathbf{r}) \rangle = \int_{\mathcal{R}^3} \mathcal{P}(\mathbf{r}) \mathcal{Q}(\mathbf{r}) \mathrm{d}\mathbf{r}$$

defines the propagator distance metric. Here we propose to generalize NG to outer 'energy levels', in order to isolate and quantify high-frequency (e.g. kink-like) features of the diffusion propagator:

$$Nr = \sqrt{1 - \frac{\langle \mathcal{P}_r, \mathcal{P}_{N_{\max}} \rangle}{\langle \mathcal{P}_{N_{\max}}, \mathcal{P}_{N_{\max}} \rangle}}$$

.
With the above notation, $NG = N0$.
Additionally, we consider a metric given by the difference between the $N0$ of the full propagator and the $N0$ of its isotropic part.

FAST PA ESTIMATION

In the original MAP-MRI method[1], estimation of propagator anisotropy (PA) with MAP-MRI required two estimations, with anisotropic and isotropic scale tensors. By setting the propagators represented in the two bases equal to each other and exploiting the orthogonality relations, we were able to show that the PA can be computed using

$$a_{m_1m_2m_3} = \sum_{N=0}^{N_{\max}} \sum_{\{n_1,n_2,n_3\}} c_{m_1n_1}(u_x, v_x)\, c_{m_2n_2}(u_y, v_y)\, c_{m_3n_3}(u_z, v_z)\, b_{n_1n_2n_3}$$

,
with

$$c_{mn}(u, v) = \frac{1}{(2^{m+n-1}\, m!\, n!(1+\lambda^2))^{1/2}} \left(\frac{\partial^m}{\partial s^m} \frac{\partial^n}{\partial t^n} e^{\frac{2(\lambda\, s+t)^2}{1+\lambda^2} - s^2 - t^2} \right) \Big|_{s=t=0}$$

where $\lambda = v/u$, and $a_{m_1m_2m_3}$ and $b_{n_1n_2n_3}$ are the coefficients in the two reference frames defined by u_x, u_y, u_z and v_x, v_y, v_z, respectively.

Methods

To determine whether enforcing the strict positivity constraints reduces the demand on the data acquisition, we analyzed a dataset from the Human Connectome Project[11] (HCP) containing a total of 288 diffusion measurements. Data were sequentially removed from the stack to simulate progressively shorter acquisition times, leading to subsampled datasets with 180, 90, 60, 50, and 40 measurements for experiments with radial order = 6, and datasets comprising 180, 150, 120, 95, 90, and 60 measurements for experiments with radial order = 8. Results on the complete dataset were considered as gold standard. For comparison, we estimated the MAP-MRI parameters for all datasets with the original method described in [1] (referred to as MAP) and the strictly constrained version described in [9] (referred to as MAP+). Both implementations are available in Dipy[12].
The novel metrics described in the theory section, as well as the fast PA, were computed on the MGH1010 dataset from the HCP[13].

Results & Discussion

Figures 1, 2, and 3 depict the NG and RTOP maps estimated using MAP and MAP+ on the subsampled datasets for radial order 6 and 8. The results obtained with MAP+ show clear tissue contrast and are robust to downsampling without requiring additional regularization techniques[14]. These findings are consistent with those obtained by incorporating strict constraints into other dMRI techniques[15,16]. The possibility of performing the estimation on a minimum number of diffusion encodings, i.e., the total number of coefficients, marks a step forward towards MAP-MRI's widespread clinical adoption for which long acquisitions are often the bottleneck.
Figure 4 shows the maps depicting the high frequency features of the propagator. Interesting contrasts emerge through the different energy levels, especially around the interface between different tissues, possibly indicating sensitivity to microstructural heterogeneity. Such contrast could be beneficial for the assessment of different diseases.
Figure 5 shows a comparison between the propagator anisotropy estimated with the conventional double fitting, and the fast method outlined in the theory section, which relies on a single fit. The results affirm the fast method as a viable clinical option, especially when the more time-consuming alternative cannot be afforded.

Conclusions

In conclusion, this work marks a step towards the clinical translation of MAP-MRI by showing that the constrained framework obviates the need for extensive data acquisition, while also providing novel tissue microstructural contrasts that may improve the detection and characterization of different diseases.

Acknowledgements

This study was supported by the Intramural Research Program (IRP) of the Eunice Kennedy Shriver National Institute of Child Health and Human Development (NICHD) and the Military Traumatic Brain Injury Initiative (MTBI2) under the auspices of the Henry M. Jackson Foundation (HJF).

References

1. Özarslan E, Koay CG, Shepherd TM, Komlosh ME, İrfanoğlu MO, Pierpaoli C, and Basser PJ. Mean apparent propagator (MAP) MRI: A novel diffusion imaging method for mapping tissue microstructure. NeuroImage, 78:16–32, September 2013.

2. Han L, Yang J, Yuan C, Zhang W, Huang Y, Zeng L, Zhong J. Assessing brain microstructural changes in chronic kidney disease: a diffusion imaging study using multiple models. Front Neurol. 2024 May 1;15:1387021. doi: 10.3389/fneur.2024.1387021.

3. Goeckner BD, Brett BL, Mayer AR, España LY, Banerjee A, Muftuler LT, Meier TB. Associations of prior concussion severity with brain microstructure using mean apparent propagator magnetic resonance imaging. Hum Brain Mapp. 2024 Jan;45(1):e26556. doi: 10.1002/hbm.26556.

4. Moody JF, Dean DC 3rd, Kecskemeti SR, Blennow K, Zetterberg H, Kollmorgen G, Suridjan I, Wild N, Carlsson CM, Johnson SC, Alexander AL, Bendlin BB. Associations between diffusion MRI microstructure and cerebrospinal fluid markers of Alzheimer's disease pathology and neurodegeneration along the Alzheimer's disease continuum. Alzheimers Dement (Amst). 2022 Dec 4;14(1):e12381. doi: 10.1002/dad2.12381.

5. Wang P, He J, Ma X, Weng L, Wu Q, Zhao P, Ban C, Hao X, Hao Z, Yuan P, Hao F, Wang S, Zhang H, Xie S, Gao Y. Applying MAP-MRI to identify the WHO grade and main genetic features of adult-type diffuse gliomas: A comparison of three diffusion-weighted MRI models. Acad Radiol. 2023 Jul;30(7):1238-1246. doi: 10.1016/j.acra.2022.10.009.

6. Avram AV, Saleem KS, Komlosh ME, Yen CC, Ye FQ, Basser PJ. High-resolution cortical MAP-MRI reveals areal borders and laminar substructures observed with histological staining. Neuroimage. 2022 Dec 1;264:119653. doi: 10.1016/j.neuroimage.2022.119653.

7. Wang P, Gao E, Qi J, Ma X, Zhao K, Bai J, Zhang Y, Zhang H, Yang G, Cheng J, Zhao G. Quantitative analysis of mean apparent propagator-magnetic resonance imaging for distinguishing glioblastoma from solitary brain metastasis. Eur J Radiol. 2022 Sep;154:110430. doi: 10.1016/j.ejrad.2022.110430.

8. Bouhrara M, Avram AV, Kiely M, Trivedi A, Benjamini D. Adult lifespan maturation and degeneration patterns in gray and white matter: A mean apparent propagator (MAP) MRI study. Neurobiology of Aging. 2023 Apr 1;124:104-16.

9. Dela Haije T, Özarslan E, and Feragen A. Enforcing necessary non-negativity constraints for common diffusion MRI models using sum of squares programming. NeuroImage, 209:116405, April 2020

10. Avram AV, Sarlls JE, Barnett AS, Özarslan E, Thomas C, Irfanoglu MO, Hutchinson E, Pierpaoli C, Basser PJ. Clinical feasibility of using mean apparent propagator (MAP) MRI to characterize brain tissue microstructure. Neuroimage. 2016 Feb 15;127:422-434. doi: 10.1016/j.neuroimage.2015.11.027.

11. Van Essen DC, Smith SM, Barch DM, Behrens TEJ, Yacoub E, Ugurbil K, for the WU-Minn HCP Consortium. (2013). The WU-Minn Human Connectome Project: An overview. NeuroImage 80(2013):62-79.

12. Garyfallidis E, Brett M, Amirbekian B, Rokem A, van der Walt S, Descoteaux M, Nimmo-Smith I and Dipy Contributors (2014). DIPY, a library for the analysis of diffusion MRI data. Frontiers in Neuroinformatics, vol.8, no.8.

13. Fan Q, Witzel T, Nummenmaa A, Van Dijk KR, Van Horn JD, Drews MK, Somerville LH, Sheridan MA, Santillana RM, Snyder J, Hedden T, Shaw EE, Hollinshead MO, Renvall V, Zanzonico R, Keil B, Cauley S, Polimeni JR, Tisdall D, Buckner RL, Wedeen VJ, Wald LL, Toga AW, Rosen BR. MGH-USC Human Connectome Project datasets with ultra-high b-value diffusion MRI. Neuroimage 2016;124(Pt B):1108-1114.

14. Fick RHJ, Wassermann D, Caruyer E, and Deriche R. MAPL: Tissue microstructure estimation using Laplacian-regularized MAP-MRI and its application to HCP data. NeuroImage, 134:365–385, July 2016.

15. Herberthson M, Boito D, Haije TD, Feragen A, Westin CF, Özarslan E. Q-space trajectory imaging with positivity constraints (QTI+). Neuroimage. 2021 Sep;238:118198. doi: 10.1016/j.neuroimage.2021.118198.

16. Boito, D., Herberthson, M., Haije, T. D., & Özarslan, E. (2021). Enforcing positivity constraints in q-space trajectory imaging (QTI) allows for reduced scan time. In Proc Intl Soc Mag Reson Med (Vol. 29, p. 0404).

Figures

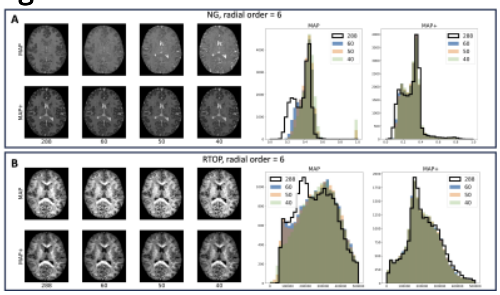

(A) Non-Gaussianity (NG) and (B) Return-to-Origin Probability (RTOP) obtained from MAP-MRI coefficients computed on the entire HCP dataset (288 measurements) and its subsampled versions for radial order = 6 using MAP and MAP+. The histograms on the right show the values' distributions. In addition to showing clearer tissue contrasts (e.g., GM/WM in NG) compared to MAP, the parameters derived using MAP+ are more consistent (e.g., GM in NG) when estimated from datasets with fewer diffusion encodings, even when the number of unknows (50) exceeds the number of diffusion measurements.

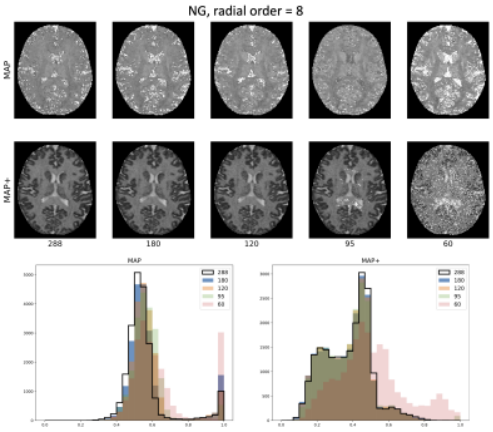

Non-Gaussianity (NG) maps obtained from MAP-MRI coefficients computed on the entire HCP dataset (288 measurements) and its subsampled versions for radial order = 8 using MAP and MAP+. The histograms on the bottom show the values' distributions. Similarly to the results for radial order = 6, the maps obtained with MAP+ exhibit clear tissue contrast and excellent consistency for smaller datasets. However, there is a clear drop in image quality when the number of unknows (95) exceeds the number of diffusion encodings.

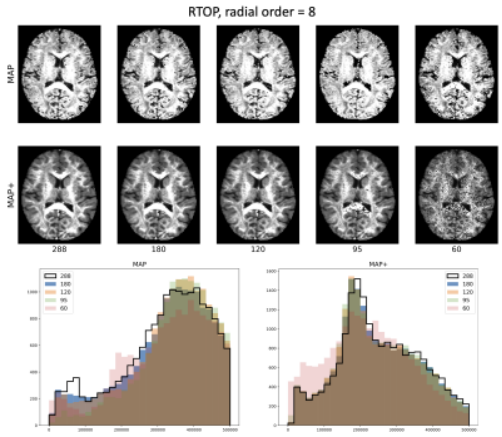

Return-to-Origin Probability (RTOP) maps obtained from MAP-MRI coefficients computed on the entire HCP dataset (288 measurements) and its subsampled versions for radial order = 8 using MAP and MAP+. The histograms on the bottom show the values distributions. Similarly to the results in Figure 2, the maps obtained with MAP+ exhibit clear tissue contrast and excellent consistency for smaller datasets, but lower image quality is observed when the number of unknows (95) exceeds the number of measurements.

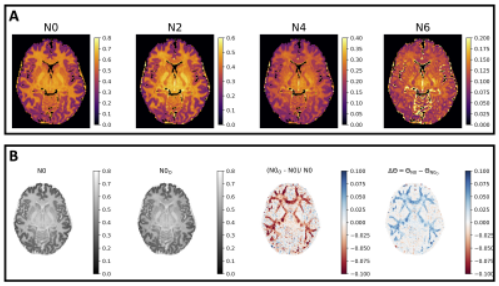

Novel metrics computed on the MGH1010 dataset using MAP+ with radial order 8. (A) The Nr maps showing the power at each 'energy shell,' which contain progressively 'higher-frequency' features of the mean propagator. In N6, high values are found at the interface between tissue types, possibly indicating sensitivity to tissue heterogeneity. (B) The difference and angular distance $\Delta\Theta$ between the NG of the full propagator (N0) and the NG of its isotropic part ($N0_o$), which seems to reveal regions presenting unidirectional diffusion

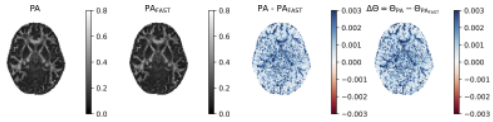

Comparison between the propagator anisotropy obtained by standard double fitting (PA) and the fast method described in the theory section which relies on single fitting (PA_{FAST}). The red-blue maps on the right side show the difference and angular difference between the two. The results highlight the overall consistency between the two methods, suggesting the fast strategy as a reliable alternative.